PHYSICAL REVIEW B **88**, 195413 (2013)

Photon energy dependence of circular dichroism of the Au(111) surface state

M. Ärrälä,[1,*] J. Nieminen,[1] J. Braun,[2] H. Ebert,[2] and M. Lindroos[1]

[1]*Institute of Physics, Tampere University of Technology, P.O. Box 692, FIN-33101 Tampere, Finland*

[2]*Department Chemie, Ludwig-Maximilians-Universität München, Butenandtstr. 5-13, D-81377 München, Germany*

(Received 13 June 2013; published 13 November 2013)

Through relativistic photoemission calculations for the Au(111) surface state at the Fermi level, we study the photon energy dependence of circular dichroism. The dichromatic signal (D_S) pattern changes 23 times with photon energies between 7 and 100 eV, and we have found 13 different patterns in the $k_\parallel$ map at the Fermi level for the D_S from the Au(111) surface state with normal incidence light. We show that the photon energy dependence of D_S is very complex even in the simplest case. The sign change in the circular dichroism as a function of photon energy is related to the relative phases of the complex expansion coefficients of different outgoing partial waves in a time-reversed low-energy electron diffraction state. With off-normal incidence, the z component of the incoming photon field is dominant, and the fine structure seen in the D_S in the normal incidence case is lost very rapidly, moving from a normal to an off-normal incidence. We also report that the Rashba split surface state of Au(111) has a significant component of d-type orbital due to relativistic effects and the computational setup used.

DOI: 10.1103/PhysRevB.88.195413 PACS number(s): 79.60.Bm, 73.20.At, 75.70.Tj

I. INTRODUCTION

In novel low-dimensional and topological materials, many fundamental properties of electronic structure arise from a relativistic origin, e.g., from variations of spin-orbit coupling (SOC). This poses new challenges to spectroscopic methods, such as angle resolved photoemission spectroscopy (ARPES), where one requires sophisticated experimental and theoretical tools in order to access finer energy scales and to probe orbital character and spin polarization in retracing the initial state of the emerging photoelectrons. Controlling the handedness of the ingoing circularly polarized light brings about the circular dichroism, which together with selection rules provides a handle to distinguish between certain special features that are split due to a broken symmetry by, e.g., SOC.

Schönhense has investigated the origin of circular dichroism in angular distribution (CDAD) in the case of grazing incidence.[1] He derived nonrelativistic theoretical expressions for CDAD from free atoms, adsorbed molecules, and clean surface of graphite. In the case of graphite, only a p_z-type initial state was considered, and thus the expression for the CDAD remains quite simple. Schönhense associated the angular dependence of the D_S to the relative phase differences between two outgoing partial waves with the same quantum number l. Fecher[2] and Fecher *et al.*[3] have done similar studies, where the angular dependence of the D_S has been investigated.

Instead of less known and more involved novel materials, we choose the relatively simple and widely studied Au(111) as a model system for determining the origin of the dependence of D_S on photon energy. Especially, the splitting of the surface state has been studied by LaShell *et al.*,[4] Reinert *et al.*,[5] Nicolay *et al.*[6] and also in Refs. 7 and 8. Guided by the existing experimental observations, we scrutinize the D_S as a function of photon energy with normal and off-normal incidence of light.

Studying normal incidence of light with p_z-type initial states readily requires relativistic calculations, as the nonrelativistic analysis provides vanishing CDAD. In the present calculations, the ARPES intensity is calculated in a fully relativistic way by utilizing the Dirac equation. For the photoemission process, the one-step model and multiple scattering theory are utilized. The surface potential is modeled using the Rundgren-Malmström barrier.[9] Although the spectra have been calculated with a fully relativistic code, the results are analyzed using the nonrelativistic theory, where relativistic terms are explicitly expressed as separate terms. The purpose of this is to make the role of relativistic effects more transparent.

We relate the change of the sign in the D_S as a function of photon energy to the zeros of the D_S. We develop a toy model for the D_S, starting from the one-step model for the ARPES intensity, and use it to search the origin of the zeros of the normalized dichromatic signal (D_N). We show that the photon energy dependence of D_N can be associated with the relative phases of the complex expansion coefficients of different outgoing partial waves. Our study also shows that, due to relativistic effects and normal incidence of light, there is a significant initial state d-type contribution to the photoemission intensity from the Au(111) Rashba split surface state.

II. THEORY

A. Photoemission intensity

In the one-step model,[10] the ARPES intensity for photoelectrons with energy ϵ_f and momentum $\mathbf{k}_\parallel$ can be expressed according to Caroli *et al.*,[11]

$$I(\mathbf{k}_\parallel,\epsilon_f) = -\frac{1}{\pi}\Im\langle \mathbf{k}_\parallel,\epsilon_f|G_2^+\Delta G_1^+\Delta^\dagger G_2^-|\mathbf{k}_\parallel,\epsilon_f\rangle. \quad (1)$$

Here, $G_2^\pm$ and G_1^+ denote the retarded (G^+) and advanced (G^-) single-particle Green's functions for the electron (G_2) and for the hole (G_1). The final state is expressed as a time-reversed low-energy electron diffraction (LEED) state, $|\Psi_f\rangle = G_2^-|\mathbf{k}_\parallel,\epsilon_f\rangle$. Using spectral function representation,

$$-\frac{1}{\pi}\Im G_1^+ = \sum_i B_{ii}|\Psi_i\rangle\langle\Psi_i|, \quad (2)$$

where the Green's function for the photohole is written as a sum (integral over k_z for all bands) of spectral functions B_{ii} over initial states. The ARPES intensity can now be expressed formally as a product of the spectral function and the matrix elements:

$$I(\mathbf{k}_\parallel,\epsilon_f) = \sum_i B_{ii} |\langle \Psi_f | \Delta | \Psi_i \rangle|^2. \tag{3}$$

The operator Δ mediates the coupling to the electromagnetic field,

$$\Delta = \frac{e}{2mc}(\mathbf{A}\cdot\mathbf{p} + \mathbf{p}\cdot\mathbf{A}) - e\Phi + \frac{e^2}{2mc^2}\mathbf{A}\cdot\mathbf{A}, \tag{4}$$

where $\mathbf{p}$ is the momentum operator, and $\mathbf{A}$ denotes the vector and Φ the scalar potentials, respectively. Applying the Coulomb gauge, $\nabla\cdot\mathbf{A} = 0$, assuming $\Phi = 0$ and neglecting the term $\mathbf{A}\cdot\mathbf{A}$, one ends up to the dipole approximation for the interaction operator:

$$\Delta \approx \frac{\mathbf{A}\cdot\mathbf{p}}{c} = \frac{i\omega\mathbf{A}\cdot\mathbf{r}}{c}. \tag{5}$$

Here atomic units $e = \hbar = m = 1$ are used.

B. Dichromatic signal

The D_S is defined as the difference between the intensities excited with right- and left-handed polarized light

$$D_S = I_{RCP} - I_{LCP}. \tag{6}$$

Using Eq. (3), the expression for the D_S in the sample's coordinate becomes[12]

$$D_S = -\frac{a^2}{2c^2}\sum_i B_{ii}\Im\{\cos\phi\sin\theta M_{fi}^{(z)}M_{if}^{(y)} - \sin\phi\sin\theta M_{fi}^{(z)}M_{if}^{(x)} + \cos\theta M_{fi}^{(x)}M_{if}^{(y)}\}, \tag{7}$$

where $M_{if}^{(j)} = \langle\Psi_f|\hat{\mathbf{j}}\cdot\mathbf{p}|\Psi_i\rangle$, and $\hat{\mathbf{j}} = \hat{\mathbf{x}},\hat{\mathbf{y}}$, or $\hat{\mathbf{z}}$. θ and ϕ are the polar and azimuthal angles of the incoming photon, respectively, and a is the amplitude of the vector potential. Thus, with normal incidence of light, D_S simplifies to

$$D_S = -\frac{a^2}{2c^2}\sum_i B_{ii}\Im\{M_{fi}^{(x)}M_{if}^{(y)}\}. \tag{8}$$

C. Toy model for dichromatic signal

The initial and final states can be written in spherical harmonic representation, according to Schönhense[1] and Pendry,[10]

$$\Psi_i = \sum_{lm} A_{1lm}R_l(k_i r)Y_{lm}(\theta,\phi),$$
$$\Psi_f = \sum_{l'm'} A_{2l'm'}R_{l'}(k_f r)Y_{l'm'}(\theta,\phi). \tag{9}$$

Here, the complex expansion coefficients

$$A_{1lm} = |A_{1lm}|\exp(i\xi_{lm}) \quad \text{and}$$
$$A_{2l'm'} = |A_{2l'm'}|\exp(i\xi_{l'm'}) \tag{10}$$

contain the corresponding relative phases ξ_{lm} and $\xi_{l'm'}$ of the partial waves l,m and l',m'. In order to obtain the D_S with normal incidence of light, the two matrix elements in Eq. (8) have to be calculated. For $M_{if}^{(x)}$ we get

$$\begin{aligned} M_{if}^{(x)} &= \langle\Psi_f|\hat{\mathbf{x}}\cdot\mathbf{p}|\Psi_i\rangle = \langle\Psi_f|p_x|\Psi_i\rangle = \langle\Psi_f|m\frac{d}{dt}x|\Psi_i\rangle \\ &= \frac{im}{\hbar}\langle\Psi_f|[H,x]|\Psi_i\rangle = \frac{im}{\hbar}\langle\Psi_f|Hx - xH|\Psi_i\rangle \\ &= \frac{im(E_f - E_i)}{\hbar}\langle\Psi_f|x|\Psi_i\rangle = im\omega\langle\Psi_f|x|\Psi_i\rangle \\ &= im\omega\sum_{ll'}\sum_{mm'}A_{2l'm'}^* A_{1lm}\int_0^\infty r^3 dr\, R_{l'}^*(k_f r)R_l(k_i r) \\ &\quad\times\int_0^\pi \sin\theta\, d\theta\int_0^{2\pi} d\phi\, Y_{l'm'}^* S(\theta,\phi)Y_{lm}, \end{aligned} \tag{11}$$

where $S(\theta,\phi) = \sin\theta\cos\phi$. Similarly, it can be written for matrix element $M_{if}^{(y)}$, for which $S(\theta,\phi) = \sin\theta\sin\phi$ [and $M_{if}^{(z)}$, for which $S(\theta,\phi) = \cos\theta$]. Using Eq. (11) to write for the two matrix elements in Eq. (8), using $m = 1$ for the mass and simplifying the equation, we get

$$M_{if}^{(j)} = i\omega\sum_{l_j l_j'}\sum_{m_j m_j'} A_{2l_j'm_j'}^* A_{1l_j m_j} R^{(j)} D^{(j)}, \tag{12}$$

where we have used shorthand notations for the radial part

$$R^{(j)} = R_{l_j l_j'} = \int_0^{2\pi} r^3 dr\, R_{l_j'}^*(k_f r)R_{l_j}(k_i r) \tag{13}$$

and the angular part

$$D^{(j)} = D_{l_j m_j l_j' m_j'} = \int_0^\pi \sin\theta\, d\theta\int_0^{2\pi} d\phi\, Y_{l_j' m_j'}^* S(\theta,\phi)Y_{l_j m_j}. \tag{14}$$

Finally, combining Eqs. (12)–(14), we get the following form for the product of the matrix elements:

$$\begin{aligned} M_{fi}^{(x)}M_{if}^{(y)} &= -i\omega\sum_{l_x l_x'}\sum_{m_x m_x'} A_{2l_x'm_x'}A_{1l_x m_x}^* R^{(x)*}D^{(x)*}\, i\omega\sum_{l_y l_y'}\sum_{m_y m_y'} A_{2l_y'm_y'}^* A_{1l_y m_y}R^{(y)}D^{(y)} \\ &= \omega^2\sum_{l_x l_x' l_y l_y'}\sum_{m_x m_x' m_y m_y'} A_{1l_y m_y}A_{1l_x m_x}^* A_{2l_x'm_x'}A_{2l_y'm_y'}^* R^{(x)*}R^{(y)}D^{(x)*}D^{(y)} \\ &= \omega^2\sum_{l_x l_x' l_y l_y'}\sum_{m_x m_x' m_y m_y'} |A_{1l_y m_y}||A_{1l_x m_x}|\exp\left[i\left(\xi_{1l_y m_y} - \xi_{1l_x m_x}\right)\right]|A_{2l_x'm_x'}||A_{2l_y'm_y'}|\exp\left[i\left(\xi_{2l_x'm_x'} - \xi_{2l_y'm_y'}\right)\right]R^{(xy)}D^{(xy)}, \end{aligned} \tag{15}$$

where $R^{(xy)} = R^{(x)*}R^{(y)}$ is a slowly varying function and $D^{(xy)} = D^{(x)*}D^{(y)}$. Equation (15) can be used to analyze the initial and final state effects on the D_S. In the present study, we follow the idea utilized by Gierz *et al*. for initial-state analysis for graphene.[13]

In the following, we apply our toy model for Au(111) surface state, where we fix the amplitude and the phase of the initial states. In our case, the initial state can be treated as a constant because we are investigating the surface state at the Fermi level for all photon energies. We have denoted $A_{1l_ym_y} = A_{1l_xm_x} = 1$ in order to study only the influence of the final states on the D_S. Hence, the difference $\xi_{1l_ym_y} - \xi_{1l_xm_x}$ in Eq. (15) is also constant and can be neglected. Considering the slow variance of $R^{(xy)}$, and treating the initial state as constant, we get for the photon energy dependence of the D_S

$$D_S \propto \Im\Bigg\{ \sum_{l_xl'_xl_yl'_y} \sum_{m_xm'_xm_ym'_y} \left|A_{2l'_xm'_x}\right|\left|A_{2l'_ym'_y}\right| \times \exp\left[i\left(\xi_{2l'_xm'_x} - \xi_{2l'_ym'_y}\right)\right] D^{(xy)} \Bigg\}, \qquad (16)$$

where $D^{(xy)}$ takes care of the dipole selection rules.

III. RESULTS

In the following, we apply fully relativistic calculations to study the dependence of the D_S on the energy of the incoming photon field. The results of the *ab initio* calculations are followed by a decomposition into different excitation channels, in order to recognize the origin of the observed variations in the D_S. Also the D_S with off-normal incidence of light has been examined, in order to test whether a photon energy dependence still exists in an off-normal setup.

A. Dichromatic signal

First, we investigate the variation of the D_S of the Au(111) surface state as a function of photon energy. In Fig. 1, the D_S at the Fermi energy in momentum space is shown. The k_x and k_y axes are aligned with the $\bar{K}$-$\bar{\Gamma}$-$\bar{K}$ and $\bar{M}$-$\bar{\Gamma}$-$\bar{M}$ lines of the two-dimensional Brillouin zone, respectively. A common feature to all photon energies is a clear splitting of the surface state due to the Rashba effect. To figure out the basic pattern of the D_S in momentum space, we start with photon energy 7 eV. At this energy, both the inner and the outer states have threefold symmetry, with the signs of D_S being the same for the inner and the outer states, which change from positive (negative) to negative (positive) every 60°. The D_S has six zeros for both Rashba split states. When increasing photon energy, the D_S changes abruptly, sometimes showing the same pattern as obtained with photon energy 7 eV. The D_S changes 23 times with photon energies in the range of 7–100 eV, and 13 different patterns of the D_S are found. Threefold symmetry applies to all photon energies due to our computational setup.

Further understanding to the nature of the D_S can be obtained by investigating different excitation channels separately. We searched for the origin of the D_S by closing excitation channels from the initial state to the final states, as Mulazzi *et al*. did with Cu(111)[14] and Scholz *et al*. with

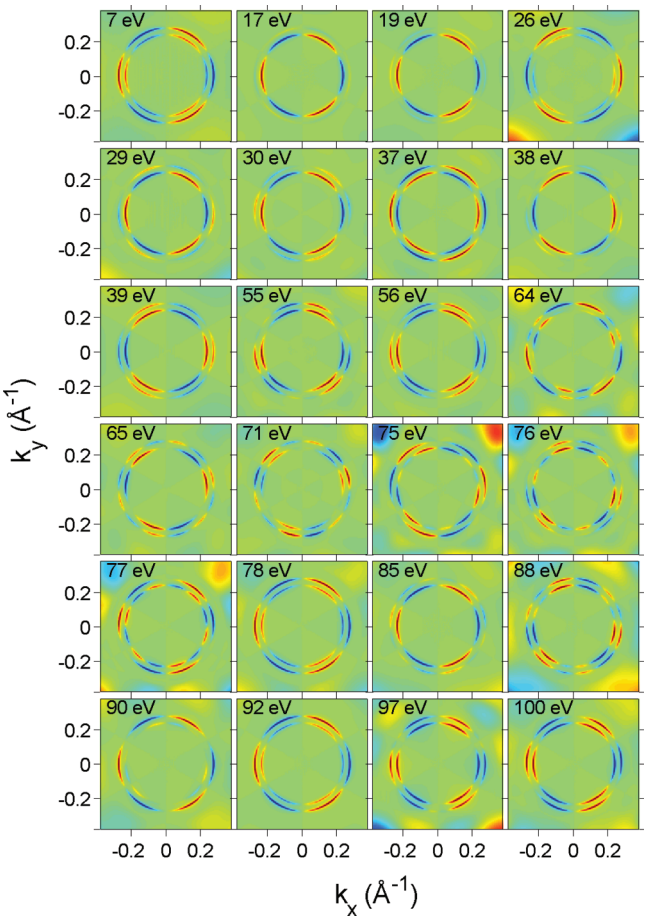

FIG. 1. (Color online) Obtained changes in the dichromatic signal with photon energies 7–100 eV. The calculations were done with normal incidence light. The blue (red) color indicates negative (positive) signal. Thirteen different patterns for the D_S are found, and the D_S changes 23 times in this photon energy range.

Bi_2Te_3.[15] We assumed that the initial state was of p_z -type, but surprisingly only minor effects were seen in the D_S and in the corresponding photoemission intensities when the channels p-to-s and p-to-d were closed. Instead, a major effect was seen when the channel d-to-f was closed. As such, our study shows that the Rashba split surface state of Au(111) has a significant d-type component and the major contribution to the photoemission intensity origins from d-type initial states when normal incidence light is used. Kim *et al*. reported that the majority of the local angular momentum of the Au(111) surface state has d-orbital origin, while a small contribution is from p-orbitals.[16] Lee and Choi investigated the role of d-orbitals in the Rashba-type spin splitting of Au(111) surface state, and they reported that, although the surface state of Au(111) is mainly p type, the Rashba-type spin splitting originates from d-type states.[17] Our investigation confirms this and also states that the main contribution to the photoemission intensity in the normal incidence setup is due to the d orbitals.

Considering Eq. (15), the radial part between the initial state and different final states varies slowly as a function of photon energy and therefore does not need to be considered when we are interested in the zeros of the D_S. In our photon energy range, the radial parts may contribute one zero to

the D_S, which is known as the Cooper minimum.[18] The Coulomb phase shifts $\delta_{l'}$—which different outgoing partial waves experience, as discussed by Schönhense[1]—are also negligible when considering the zeros of D_S.

If the expansion coefficients for the same quantum number l and opposite quantum numbers m are equal, it is possible to talk about orbitals. When considering relativistic effects, these orbitals are no longer meaningful. Strictly speaking, quantum numbers l and m are not good quantum numbers, and therefore we use the κ, μ representation. In Schönhense's model,[1] the final d-states with quantum number $m = \pm 1$ are described as orbitals having a common complex expansion coefficient. Fecher *et al.* have also used the orbital representation with common expansion coefficients.[3] In our model, final states with the same quantum number l and opposite quantum numbers m cannot be combined together in a similar way because the complex expansion coefficients—for example the coefficients for $l = 1, m = \pm 1$—are unequal, and thus we need to have separate coefficients for both states.

B. Origin of the zeros in the D_S as a function of photon energy

In the following, we apply our toy model to the surface state of Au(111). First, we search the important excitation channels by closing them separately and adapt those which contribute to the photoemission intensity. When closing the excitation channels to the final states with $l = 3$, $m = \pm 3$, no notable changes were seen in the photoemission intensities or in the D_S. On that account, in our toy model, the initial state is described with $l = 2$, $m = 0, \pm 1$. Considering the dipole selection rules, the final state is $l = 1$, $m = 0, \pm 1$ or $l = 3$, $m = 0, \pm 1, \pm 2$. Now, in calculating the matrix elements $M_{fi}^{(x)}$ and $M_{if}^{(y)}$ in Eq. (8), it is evident that they both contain ten terms. In carrying out the multiplication, we end up with 100 terms. By holding the initial state constant, the only factors we need to consider are the final state complex expansion coefficients $A_{2l'_x m'_x}$ and $A_{2l'_y m'_y}$, which we took from our one-step computation. The square of the absolute value of the expansion coefficient $|A_{2\kappa\mu}|^2$ is the probability amplitude of the final state, having quantum numbers κ and μ. With the coefficients taken from our one-step computation, we can determine the weights of all possible final states. In Fig. 2, the magnitude $|A_{2\kappa\mu}|$ and phase $\xi_{2\kappa\mu}$ of the relativistic expansion coefficients are shown for $\kappa = -2$ and $\kappa = 2$. For both κ values, μ gets values $\mu = -\frac{3}{2}, -\frac{1}{2}, \frac{1}{2}, \frac{3}{2}$. The magnitudes $|A_{2\kappa\mu}|$ all have strong photon energy dependence, as clearly seen in the upper panel in Fig. 2. For both κ values, $\mu = \frac{1}{2}$ has the largest value for all photon energies. In the lower panel in Fig. 2, the corresponding phases $\xi_{2\kappa\mu}$ are shown. In the photon energy range used, the phases change approximately by 30 rad for $\kappa = -2$ and 40 rad for $\kappa = 2$. Just looking at a single $\xi_{2\kappa\mu}$ value and its sine or cosine dependent contribution in the D_S, we see that one $\xi_{2\kappa\mu}$ value can produce more than 11 zeros to the D_S. It is also notable that the phases for different quantum numbers cross one another in the used photon energy range.

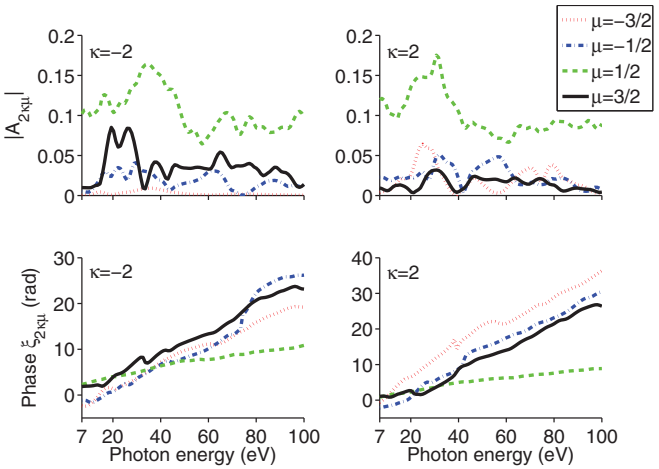

FIG. 2. (Color online) The magnitude $|A_{2\kappa\mu}|$ and phase $\xi_{2\kappa\mu}$ of the relativistic expansion coefficients obtained from our one-step calculation for $\kappa = -2$ and $\kappa = 2$

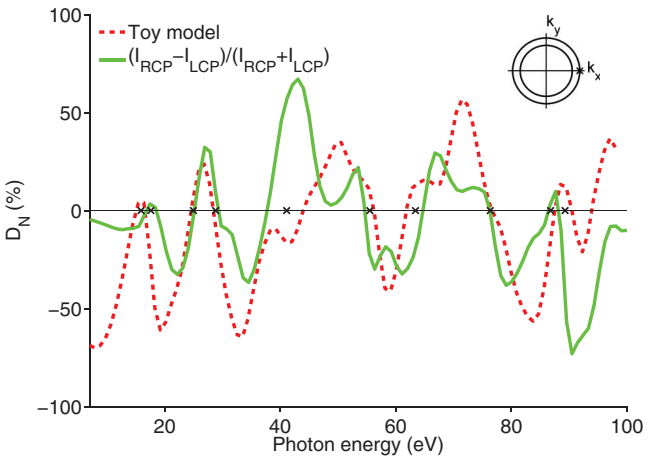

FIG. 3. (Color online) A comparison between the normalized dichromatic signal obtained with a fully relativistic one-step calculation and our toy model in a fixed $k_\parallel$ point. The marks in the x axis are a guide for the eye to notice where the calculated D_N and our toy model have their corresponding zeros.

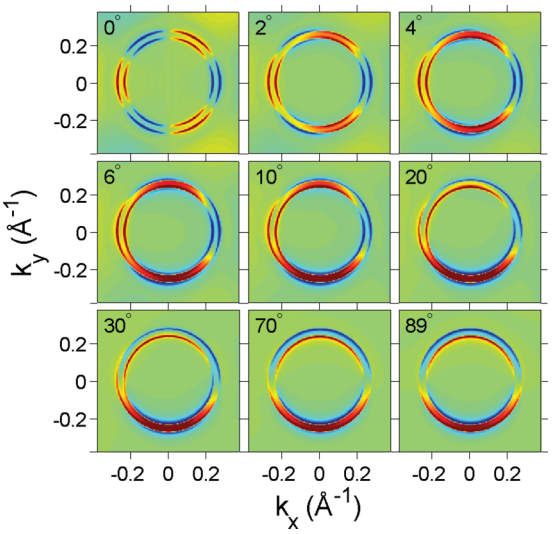

FIG. 4. (Color online) The dichromatic signal with different polar angles of the incoming photon. Photon energy is 10 eV for all polar angles. The color scaling is similar to Fig. 1. The change in the D_S happens very quickly when the polar angle is increased.

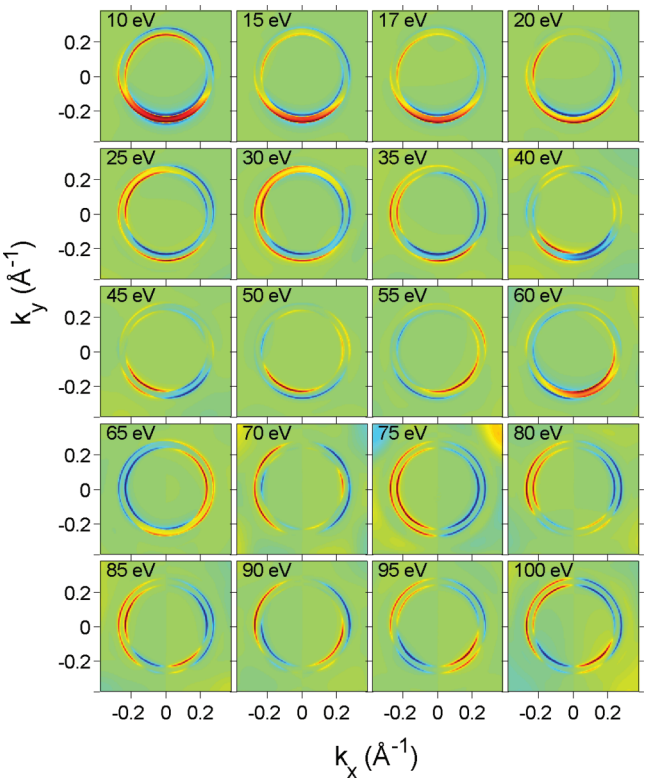

FIG. 5. (Color online) The dichromatic signal with photon angle $\theta = 30^\circ$ for different photon energies. The color scaling is similar to Fig. 1. Although the photon energy dependence is much more moderate than seen for the normal incidence setup in Fig. 1, a clear energy dependence is still evident.

The 100 terms obtained from Eq. (8) contain factors that are proportional to $\exp[i(\xi_{2l'_x m'_x} - \xi_{2l'_y m'_y})]$. Here, $\xi_{2l'_x m'_x}$ and $\xi_{2l'_y m'_y}$ are relative phase factors of two outgoing waves with different quantum numbers. In Fig. 3, a comparison between the normalized dichromatic signal $D_N = (I_{RCP} - I_{LCP})/(I_{RCP} + I_{LCP})$ from a fully relativistic one-step calculation and our toy model from Eq. (16) in a fixed $k_\parallel$ point is shown. As seen in the figure, our model picks out the zeros of the D_N almost perfectly. The D_N calculated with the intensities I_{RCP} and I_{LCP} has 10 zeros. Our toy model has one extra zero around 90 eV, although a similar structure is visible in the D_N, lying a little bit lower with respect to the x axis. Differences seen between the two graphs in the positions of the zeros are due to our approximation for the initial-state expansion coefficients and also for the selection of the possible initial and hence the final states. The difference seen in the magnitude of the D_N and our toy model is not meaningful because we are only interested in the zeros of the D_N;i.e., the change of the sign in the D_N. Similar calculations were made in different $k_\parallel$ points, and the same kind of agreement between the calculated D_N and our toy model was discovered.

C. Off-normal incidence

With off-normal incidence of light, all of the matrix elements in Eq. (7) contribute to the D_S, making it a rather complicated function. In Fig. 4, the D_S with different polar angles of the incoming photon field is shown. The photon energy is 10 eV and the azimuthal angle $\phi = 0^\circ$ for all cases. The D_S seen with normal incidence of light is very rapidly altered when moving from normal incidence to an off-normal incidence setup. With polar angle $\theta = 4^\circ$, the pattern seen in the normal incidence case is still visible, but the separately seen Rashba split states begin to get blurry. This effect is due to the z component of the incoming photon field, which appears to dominate the photoemission process. This strong polar angle dependence results in high requirements for experimental measurements. When changing from normal incidence to off-normal incidence setup, the z component of the incoming photon field A_z increases as the polar angle increases, and the terms in Eq. (7) with matrix element $M_{fi}^{(z)}$ determine the D_S. To test whether the photon energy dependence still exists in an off-normal setup, we calculated the D_S with photon angles $\theta = 30^\circ$, $\phi = 0^\circ$ for different photon energies. The obtained results are shown in Fig. 5. As seen in the figure, with off-normal incidence of light, the multiple patterns of the D_S seen in the normal incidence setup in Fig. 1 are lost, and variation of the D_S as a function of photon energy is much more moderate, but a clear photon energy dependence is still evident.

IV. CONCLUSIONS

Our investigation shows that the photoemission intensity from the Rashba split surface state of Au(111) in a normal incidence setup originates mainly from d-type orbitals due to the relativistic effects. We have also shown that the zeros of the D_S as a function of photon energy are related to the relative phase differences between different outgoing partial waves. Excluding different excitation channels suggest that the initial states with quantum numbers $l = 2, m = 0, \pm 1$ give the dominant contribution to the D_S. Applying the dipole selection rules and our toy model with fixed amplitude and phase for the initial state, we end up to a toy model with 100 terms. This model gives a very good description of the D_S, and leads to an excellent match for the zeros of the D_S as compared to a fully relativistically calculated spectra. Hence, the factor determining the change of the sign of the D_S is the relative phase between the different outgoing partial waves.

ACKNOWLEDGMENTS

This work benefited from grid computing software provided by Techila Technologies Ltd and was supported by the Deutsche Forschungsgemeinschaft (Grants No. SPP 1666 and No. EBE-154/23-1).

*minna.arrala@tut.fi

[1] G. Schönhense, Phys. Scr. **31**, 255 (1990).
[2] G. H. Fecher, Europhys. Lett. **29**, 605 (1995).
[3] G. Fecher, V. Kuznetsov, N. A. Cherepkov, and G. Schönhense, J. Electron Spectrosc. Relat. Phenom. **122**, 157 (2002).

[4]S. LaShell, B. A. McDougall, and E. Jensen, Phys. Rev. Lett. **77**, 3419 (1996).
[5]F. Reinert, G. Nicolay, S. Schmidt, D. Ehm, and S. Hüfner, Phys. Rev. B **63**, 115415 (2001).
[6]G. Nicolay, F. Reinert, S. Hüfner, and P. Blaha, Phys. Rev. B **65**, 033407 (2001).
[7]M. Hoesch, M. Muntwiler, V. N. Petrov, M. Hengsberger, L. Patthey, M. Shi, M. Falub, T. Greber, and J. Osterwalder, Phys. Rev. B **69**, 241401 (2004).
[8]A. Nuber, J. Braun, F. Forster, J. Minár, F. Reinert, and H. Ebert, Phys. Rev. B **83**, 165401 (2011).
[9]G. Malmström and J. Rundgren, Comput. Phys. Commun. **19**, 263 (1980).
[10]J. Pendry, Surf. Sci. **57**, 679 (1976).
[11]C. Caroli, D. Lederer-Rozenblatt, B. Roulet, and D. Saint-James, Phys. Rev. B **8**, 4552 (1973).
[12]V. Arpiainen, V. Zalobotnyy, A. A. Kordyuk, S. V. Borisenko, and M. Lindroos, Phys. Rev. B **77**, 024520 (2008).
[13]I. Gierz, M. Lindroos, H. Höchst, C. R. Ast, and K. Kern, Nano Lett. **12**, 3900 (2012).
[14]M. Mulazzi, G. Rossi, J. Braun, J. Minár, H. Ebert, G. Panaccione, I. Vobornik, and J. Fujii, Phys. Rev. B **79**, 165421 (2009).
[15]M. R. Scholz, J. Sánchez-Barriga, J. Braun, D. Marchenko, A. Varykhalov, M. Lindroos, Y. J. Wang, H. Lin, A. Bansil, J. Minár, H. Ebert, A. Volykhov, L. V. Yashina, and O. Rader, Phys. Rev. Lett. **110**, 216801 (2013).
[16]B. Kim, C. H. Kim, P. Kim, W. Jung, Y. Kim, Y. Koh, M. Arita, K. Shimada, H. Namatame, M. Taniguchi, J. Yu, and and C. Kim, Phys. Rev. B **85**, 195402 (2012).
[17]H. Lee and H. J. Choi, Phys. Rev. B **86**, 045437 (2012).
[18]J. W. Cooper, Phys. Rev. **128**, 681 (1962).